Electron cooling in decaying low-pressure plasmas

Yusuf Celik,[1,*] Tsanko V. Tsankov,[1] Mitsutoshi Aramaki,[2] Shinji Yoshimura,[3] Dirk Luggenhölscher,[1] and Uwe Czarnetzki[1]

[1]*Institute for Plasma and Atomic Physics, Ruhr University Bochum, 44780 Bochum, Germany*

[2]*Department of Electrical Engineering and Computer Science, Nagoya University, Nagoya 464-8603, Japan*

[3]*National Institute for Fusion Science, Toki 509-5292, Japan*

(Received 10 October 2011; revised manuscript received 17 February 2012; published 9 April 2012)

A simple analytical fluid dynamic model is developed for evaporative electron cooling in a low-pressure decaying plasma and compared to a two-dimensional simulation and experimental data for the particular case of argon. Measured electron temperature and density developments are fully reproduced by the *ab initio* model and the simulation. Further, it is shown that in the late afterglow thermalization of electrons occurs by coupling to the ion fluid via Coulomb collisions at sufficiently high electron densities and not by coupling to the neutral background.

DOI: 10.1103/PhysRevE.85.046407 PACS number(s): 52.20.−j, 52.25.Fi, 52.50.Sw, 52.65.Kj

I. INTRODUCTION

Diffusional or evaporative cooling—the diffusional losses of predominantly high-energy particles—is a ubiquitous phenomenon ranging from star escape in globular clusters [1] to very effective cooling of trapped atoms, permitting Bose-Einstein condensation [2–4], and last but not least, evaporation of fluids, of course. In low-pressure plasmas it was first observed in the 1950s [5] as an efficient means to cool electrons in the afterglow. Naturally, the process is particularly important for pulsed plasma applications where the cold afterglow has recently moved again into the focus of current research [6,7]. In contrast to the importance of the process, only little work was done on the theoretical description, including numerical integration of the Boltzmann equation [7] and fluid modeling [8] based on some ad hoc assumptions.

Generally, there is a close connection to the familiar energy, momentum, and particle balance governing stationary plasmas. However, the rather cold electron temperature leads to new effects that make the situation rather distinct. While evaporation of a liquid provides the analogy for cooling of a plasma by electron loss to the wall, some remarkable differences exist. In a decaying plasma, the "work function" that energetic electrons have to overcome when escaping from the system (evaporation) is a function of the electron temperature. Furthermore, the diffusional transport from the bulk to the boundary depends on the electron and the ion temperature. Moreover, thermalization of the electrons occurs by Coulomb collisions with the ions and not by elastic collisions with the neutrals. The physics of this process is investigated by an analytical model, which provides a simple quantitative prediction of the energy and particle decay rates. This model is compared to a substantially more complex two-dimensional (2D) simulation which avoids the necessary simplification made in the analytical model. Both model and simulation are compared to an experiment where electron temperature and density are measured temporally resolved. The paper is structured accordingly.

II. ANALYTICAL MODEL

Calculation of the electron mean energy in the afterglow starts with the second moment of the Boltzmann equation:

$$\frac{\partial}{\partial t}(n_e\langle\varepsilon\rangle) + \vec{\nabla}\cdot(n_e\langle\varepsilon\vec{v}\rangle) = -\vec{j}\cdot\vec{\nabla}\Phi - 2\frac{m_e}{m_i}\nu n_e\left(\langle\varepsilon\rangle - \frac{3}{2}kT_g\right). \quad (1)$$

Here, n_e, ε are the electron density and energy, $\vec{j}$ the electron current density, Φ the electrostatic potential, $m_{e,i}$ the electron and ion mass (equal to the neutral mass), and $3/2\,kT_g$ the mean energy of the background gas or ion particles. Since ions and neutrals exchange energy very efficiently, they are assumed to be equithermal at all times. The brackets stand for an averaging over the electron energy distribution function (eedf). The energy flux density $n_e\langle\varepsilon\vec{v}\rangle$, $\vec{v}$ being the particle velocity, consists of a convective part and a conductive part, i.e., the heat flux $\vec{q}$. On the right-hand side only thermalizing collisions are taken into account. Inelastic collisions (ionization, excitation) become negligible on a time scale very short compared to the electron cooling time. $\nu = \nu_{ei} + \nu_{en}$ is the sum of the electron-ion and electron-neutral collision frequencies.

Major assumptions in the analytical model are (a) a Maxwellian eedf and (b) a spatially homogeneous temperature T_e. Rapid thermalization via electron-electron Coulomb collisions at low temperatures and relatively high densities motivates (a). In fact, temporally resolved measurements performed under similar conditions [8,9] show that an initial Druyvesteyn-like distribution relaxes to a Maxwell-like distribution within the characteristic time for cooling τ_ε (to be defined below). A perturbative approach to (1) shows that the electron temperature becomes homogeneous on the time scale of the electron diffusion time, which is much shorter than both the ambipolar diffusion time and the energy decay time. This argument is confirmed by the simulation allowing for gradients. Then $\langle\varepsilon\rangle = 3/2\,kT_e$, $n_e\langle\varepsilon\vec{v}\rangle = 5/2\,kT_e n_e\vec{u}$, $\vec{\nabla}T_e = 0$, and $\vec{q} = 0$ with $\vec{u} = \langle\vec{v}\rangle$.

Homogeneity of T_e allows volume averaging of (1):

$$\frac{k\dot{T}_e}{kT_e} = -\frac{2}{3}\frac{A}{V}\frac{1}{\langle n_e\rangle_V}\left\langle(\vec{\sigma}\cdot\vec{\Gamma}_e)\left(1+\frac{e\delta\Phi}{kT_e}\right)\right\rangle_A - \frac{\langle\Sigma\rangle_V}{kT_e}. \quad (2)$$

*Yusuf.Celik@rub.de

The dot represents the temporal derivative, $\vec{\sigma}$ is the normal vector pointing outward to the walls, and $\langle\Sigma\rangle_V = 2(m_e/m_i)\langle\nu\rangle_V k(T_e - T_g)$ is the collisional contribution, with k being the Boltzmann constant and T_g the gas temperature. The volume integral is carried out by making use of the continuity equation. This eventually leads to an averaging of the potential in the bulk weighted by the time derivative of the electron density distribution. As a very good approximation, in this step the value for the potential is replaced by the maximum in the center (see Appendix A). The subscripts A and V indicate surface and volume averaging. For equipotential (conducting) walls the potential difference between the center and the wall $\delta\Phi$ is constant and the surface averaging applies only to $(\vec{\sigma}\cdot\vec{\Gamma}_e)$.

Globally the charge particle fluxes balance: $\langle\vec{\sigma}\cdot\vec{\Gamma}_e\rangle_A = \langle\vec{\sigma}\cdot\vec{\Gamma}_i\rangle_A$. The local ion flux at the wall equals the ambipolar diffusion flux at the edge with the ambipolar diffusion constant $D_a = (kT_e + kT_i)/m_i\nu_{in}$, where ν_{in} denotes the ion-neutral collision frequency. It is assumed that the plasma is in the fundamental diffusion mode $n_e^{(0)}$ at all times:

$$\frac{\langle\vec{\sigma}\cdot\vec{\Gamma}_e\rangle_A}{\langle n_e\rangle_V} = \frac{\langle\vec{\sigma}\cdot\vec{\Gamma}_i\rangle_A}{\langle n_e\rangle_V} = -D_a\frac{\langle\vec{\sigma}\cdot\vec{\nabla}n_e^{(0)}\rangle_A}{\langle n_e^{(0)}\rangle_V}. \tag{3}$$

In the analytical model, a cube geometry with an edge length L and a classical cosine diffusion profile are assumed:

$$n_e(\vec{r},t) = n_c(t)\cos\left(\pi\frac{x}{L}\right)\cos\left(\pi\frac{y}{L}\right)\cos\left(\pi\frac{z}{L}\right), \tag{4}$$

where n_c is the maximum center electron density. Then $\langle n_e\rangle_V = n_c 8/\pi^3$ and $\langle\vec{\sigma}\cdot\vec{\Gamma}_e\rangle_A = 4n_c D_a/L\pi$.

The potential difference between the center and the walls $\delta\Phi$ is determined by the global charged particle flux balance which is evaluated by using the Boltzmann factor $n_w = n_c\exp(-\delta\Phi/kT_e)$ and the thermal flux $\vec{\sigma}\cdot\vec{\Gamma}_e = v_{th}n_w/4$ for electrons at the walls, where $v_{th} = \sqrt{8kT_e/\pi m_e}$ represents the thermal velocity and n_w the electron density at the wall.

Inserting these results in Eq. (2), the electron temperature equation is derived:

$$\frac{k\dot{T}_e}{kT_e} = -2D_a\left(\frac{\pi}{L}\right)^2\left[2 + \ln\left(\frac{Lv_{th}}{16D_a}\right) \pm c_w\right] - \frac{\langle\Sigma\rangle_V}{kT_e}. \tag{5}$$

The positive sign in front of $c_w = \ln(\pi) - 1 \ll 1$ corresponds to the above case of conducting walls. Carrying out a similar calculation for dielectric walls (local flux balance) gives the negative sign. The calculation is provided in Appendix B.

Expanding the first term by $D_a^{(0)}$—the initial diffusion constant with $kT_e^{(0)}$—the cooling time constant τ_ε can be identified as

$$\frac{1}{\tau_\varepsilon} = 2D_a^{(0)}\left(\frac{\pi}{L}\right)^2\left[2 + \ln\left(\frac{Lv_{th}^{(0)}}{16D_a^{(0)}}\right)\right]. \tag{6}$$

In the logarithm, kT_e is approximated by its initial value $kT_e^{(0)}$, which is justified over a wide range due to the weak functional dependence. Furthermore, the small difference between dielectric and conducting walls is neglected. Using typical experimental conditions $\nu_{in} = 1.53\times10^5\ s^{-1}$ [10] at a neutral gas pressure of 1 Pa, $kT_e^{(0)} = 3.2$ eV, and an edge length of $L = 0.5$ m, one calculates an electron energy decay time of $\tau_\varepsilon = 30\ \mu s$.

Normalizing the time and the electron temperature [$\tau = t/\tau_\varepsilon$, $\Theta(\tau) = kT_e/kT_e^{(0)}$] and using $kT_e^{(0)} \gg kT_i^{(0)}, kT_g$, Eq. (5) takes a simple form,

$$\dot{\Theta} = -\Theta^2 - \beta\Theta - \frac{\alpha_0 n}{\Theta^{3/2}}(\Theta - \beta), \tag{7}$$

with the initial condition $\Theta(0) = 1$. The parameters are

$$\alpha_0 = C_{ei}\left(\frac{\pi}{4}\right)^3\frac{n_c^{(0)}\ln\Lambda\,\tau_\varepsilon}{\left(kT_e^{(0)}\right)^{3/2}}, \quad \beta = \frac{kT_g}{kT_e^{(0)}} \ll 1. \tag{8}$$

$n(\tau) = n_c(\tau)/\,n_c^{(0)}$ is the electron center density normalized to its initial value, $\ln\Lambda \approx 6$ is the Coulomb logarithm, and $C_{ei} = 7.4\times10^{-17}\ eV^{3/2}\,m^3\,s^{-1}$ [11]. Under our experimental conditions typical values of α_0 are of the order of 10^{-4}. Comparison of the thermalizing rates leads to the conclusion that Coulomb collisions dominate elastic collisions at room temperature if $\nu_{en}/n_e < 10^{-9}\ m^3\,s^{-1}$. For argon at a plasma density of $10^{17}\ m^{-3}$, this is fulfilled for pressures up to 100 Pa.

For $1 > \Theta > \beta$, the collisional term can be neglected. The resulting Bernoulli differential equation has the solution

$$\frac{\beta}{\Theta} = (1+\beta)e^{\beta\tau} - 1. \tag{9}$$

For $\beta\tau \ll 1$, the exponential can be expanded, leading to $\Theta = (1+\tau)^{-1}$ with $\beta \ll 1$. This hyperbolic regime corresponds to the electron-temperature-dominated diffusional decay ($\dot{\Theta} \approx -\Theta^2$). In case that $\beta\tau \gg 1$, the electron temperature exhibits an exponential decrease corresponding to an ion-temperature-dominated diffusional decay ($\dot{\Theta} \approx -\beta\Theta$).

The diffusive density decay is calculated using the diffusional density profile and the continuity equation:

$$\dot{n} = -\gamma(\Theta + \beta)n. \tag{10}$$

The constant γ is defined by the ambipolar diffusional time constant in the stationary case $\tau_d^{(0)}$:

$$\gamma = \frac{\tau_\varepsilon}{\tau_d^{(0)}} = \tau_\varepsilon\frac{D_a^{(0)}}{l_d^2}. \tag{11}$$

The diffusional length l_d is calculated from the above cosine profile as $l_d = L/(\sqrt{3}\pi) = 0.092$ m. Note that $1/\gamma$ is 2/3 of the term in the square brackets in (6), which is only weakly dependent on the initial electron temperature. Here $\gamma = 0.17$.

Taking (9) into account, the solution of Eq. (10) is $n = \Theta^\gamma$. Since $\gamma \ll 1$, it becomes apparent that the electron temperature decreases faster than the density.

When the electron temperature approaches the gas temperature, thermalizing Coulomb collisions become significant and the temperature decay slows down substantially. Assuming an adiabatic variation with density ($\dot{\Theta} \approx 0$) in Eq. (7) one obtains

$$\alpha_0 n = -\Theta^{5/2}\frac{\Theta/\beta + 1}{\Theta/\beta - 1}. \tag{12}$$

When $\Theta \ll \beta$ this equation reduces to $n \approx \Theta^{5/2}/\alpha_0$. In contrast to the above behavior, now the density decays much faster than the temperature. In this sense, evaporation cooling of electrons is only efficient above the gas temperature. Similarly, the continuity equation reduces to $\dot{n} \approx -\gamma\beta n$, with the solution $n \propto \exp(-\gamma\beta\Delta\tau)$ where $\Delta\tau = (\tau - \tau_\beta)$. As a rough estimation, an extension of these solutions to $\Theta \approx \beta$ is

assumed. Then for $\Theta < \beta$,

$$\frac{\beta}{\Theta} \approx \exp\left(\frac{2}{5}\gamma\beta\Delta\tau\right). \tag{13}$$

The time τ_β can be estimated from Eq. (9) as $\tau_\beta = \ln(2)/\beta \approx 1/\beta$. Therefore, for low temperatures, the decay should behave approximately exponentially with a characteristic decay time of $5/2\ m_i \nu_{in} l_d^2/kT_i$, i.e., 5/2 times larger than the diffusional decay time at the ion temperature.

III. SIMULATION

The numerical 2D simulation in cylindrical geometry is based on Eq. (1), and the ambipolar diffusion equation for the charged particle density n_+. The diffusion equation is

$$\frac{\partial n_+}{\partial t} + \vec{\nabla}\cdot(-D_a\vec{\nabla}n_+) = \frac{\delta n_+}{\delta t}. \tag{14}$$

The model further includes the continuity equation for the densities of the excited argon atoms in the two metastable states—$1s_3$ and $1s_5$ in Paschen notation, denoted as N_3 and N_5, respectively:

$$\frac{\partial N_{3,5}}{\partial t} + \vec{\nabla}\cdot(-D_{3,5}\vec{\nabla}N_{3,5}) = \frac{\delta N_{3,5}}{\delta t}. \tag{15}$$

The source and sink terms on the right-hand side include: for the diffusion equation (14) ionization from the ground state and from the two metastable states, for the metastable atom balance (15) excitation and deexcitation from and to the ground state, and coupling between the first four levels of the argon atom by electron impact, and for the electron energy balance (1) losses due to ionization, energy gain and losses due to collisions, as well as work in the ambipolar field. Further, an external heating term is added to Eq. (1) to account for (pulsed) inductive power input. Penning ionization is also included in the energy and particle balances. In Table I the processes included in the simulation are summarized. The corresponding rate constants are obtained by integrating the cross sections [12] over a Maxwellian distribution function. The rate constants for the reverse processes are obtained by detailed balance. The mobility coefficient is taken from [10]. In contrast to the analytical model, the gas temperature ($T_g = T_i$) is not homogeneous but the profile is calculated self-consistently for the steady state and then kept constant in the afterglow. The simulation also includes possible heating by superelastic collisions with metastables [13]. It is found that this contribution does not play a role under our conditions. Sheaths are not explicitly included but are considered as a boundary condition for the energy balance equation by the floating potential $\delta\Phi_{sh}$:

$$\vec{\sigma}\cdot(n_e\langle\varepsilon\vec{v}\rangle) = \left(\frac{5}{2}kT_e + e\delta\Phi_{sh}\right)n_+u_B. \tag{16}$$

The boundary condition for the diffusion equation is the Bohm flux [14]. Furthermore, the diffusional flux of metastables at the boundary is equal to one half of their thermal flux:

$$-D_{3,5}(\vec{\sigma}\cdot\vec{\nabla}N_{3,5}) = \tfrac{1}{2}v_{th}N_{3,5}. \tag{17}$$

The simulation is realized with COMSOL by first obtaining the steady-state solution and then solving the time-dependent problem where the external heating is switched off. Conditions are identical to the experiments.

IV. RESULTS AND DISCUSSION

To verify the model an experiment was carried out in an inductively coupled plasma at 1 Pa neutral gas pressure and 1 kW applied radio-frequency (rf) power [21]. The cylindrical discharge vessel is approximately 0.5 m in height and in diameter, resulting in the same surface to volume ratio as a cube with $L = 0.5$ m. The rf (13.56 MHz) power is modulated at 5–20 Hz, duty cycle 85%, and applied to a flat coil antenna. The line-integrated electron density is measured by a 26.5 GHz microwave interferometer [22]. In the stationary discharge, Langmuir probe and absorption spectroscopic measurements are carried out to obtain the center electron density and the line-integrated gas temperature [21]. Time-resolved ion velocity distribution functions (ivdfs) are measured at the chamber bottom via a retarding field energy analyzer [23].

Measured ivdfs at different times upon pulse termination are shown in the inset of Fig. 1. Since the sheaths are collisionless, a monoenergetic ion distribution is found throughout. This allows deduction of the electron temperature from the peak energy E_{ion} by $kT_e = 2E_{ion}/[1 + \ln(m_i/2\pi m_e)]$. In the stationary case, very good agreement between this method and Langmuir probe measurements is found. In the main part of the figure the inverse of the normalized temperature is shown as a function of time. Very good agreement between

TABLE I. Reactions included in the numerical simulation. The index 0 represents the ground state, whereas the other indices stand for the resonant ($Ar_{2,4}$) and metastable ($Ar_{3,5}$) states.

No	Reaction	Description	Ref.
1	$e + Ar_0 \rightarrow e + e + Ar^+$	Ion formation (electron impact)	[15]
2	$e + Ar_0 \rightleftharpoons e + Ar_{3,5}$	Metastable formation (electron impact)	[12]
3	$e + Ar_{3,5} \rightarrow e + e + Ar^+$	Stepwise ionization (electron impact)	[16]
4	$e + Ar_{3,5} \rightarrow Ar_{2,4}$	Collisional transfer	[12]
5	$e + Ar_3 \rightleftharpoons e + Ar_5$	Collisional transfer, superelastic collisions	[12]
6	$e + Ar_0 \rightarrow e + Ar^{(exc)}$	Total excitation (energy)	[17]
7	$e + Ar_0 \rightarrow e + Ar_0$	Elastic collisions (energy)	[18]
8	$Ar_{3,5} + Ar_{3,5} \rightarrow Ar_0 + Ar^+ + e$	Penning ionization	[19]
9	$e + Ar^+ \rightarrow e + Ar^+$	Elastic collisions	[20]
10	$Ar_0 + Ar^+ \rightarrow Ar_0 + Ar^+$	Elastic collisions	[10]

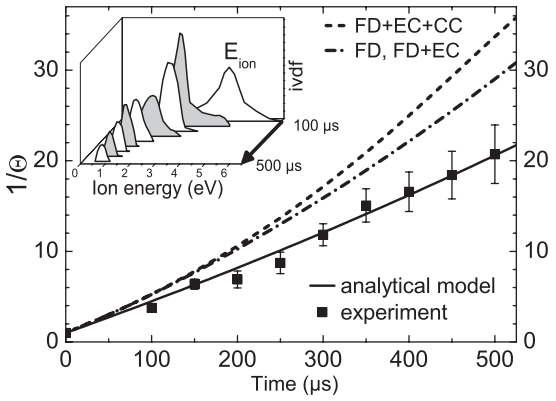

FIG. 1. Measured (squares) and simulated (dashed and dash-dotted line) temporal evolution of the inverse normalized temperature. The dash-dotted line represents simulation results including free-diffusional (FD) cooling with and without elastic collisions (ECs) as the curves for FD and FD + EC are identical. Accounting additionally for Coulomb collisions (CC) results in the dashed curve. The solid line represents an *ab initio* calculation according to Eq. (9) with $\beta = 0.017$ and $\tau_\varepsilon = 30\ \mu$s ($T_e^{(0)} = 3.2$ eV and $T_g^{(0)} = 0.055$ eV measured). The simulation gives $\langle\beta\rangle_V = 0.018\,5$ and $\tau_\varepsilon = 36\ \mu$s. The inset shows measured ivdfs as a function of time.

the experiment, the *ab initio* calculation, and the simulation is found throughout. Differences between the simulation on the one hand and the analytical model and the experiment on the other hand are mainly due to the gas temperature profile and uncertainties in the collision parameters, especially ν_{in}. Elastic collisions play a negligible role, but Coulomb collisions slightly enhance cooling, especially at later times, since the temperature of the electrons is above the ion temperature.

Figure 2 shows a remarkable agreement between the measured, the *ab initio* calculated, and the simulated temporal development of the normalized line-integrated electron density. This measurement shows that within 500 μs the

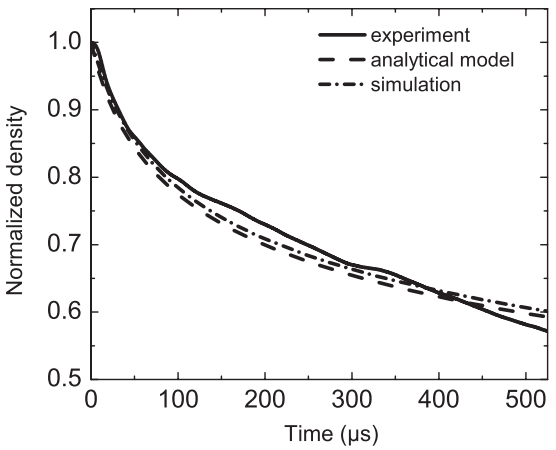

FIG. 2. Temporal development of the electron density normalized to the initial density obtained from the measurement (solid line), the simulation (dash-dotted line), and the *ab initio* calculation (dashed line, $\gamma = 0.17$) for the same conditions as in Fig. 1. The measured initial center electron density amounts to 4×10^{17} m^{-3}. The simulation provides $\gamma = 0.17$.

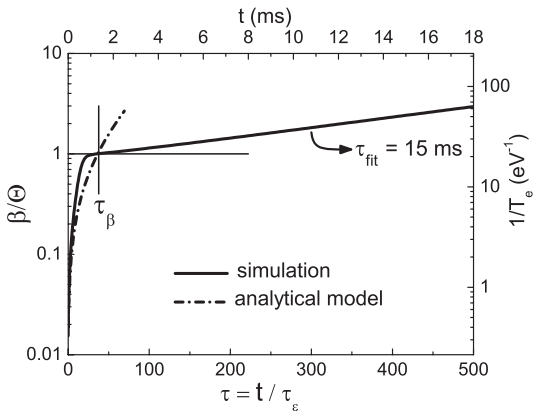

FIG. 3. Simulated (solid line) and *ab initio* calculated result for the inverse temperature decay in normalized (bottom and left scale) and natural (top and right scale) quantities on a semilogarithmic scale.

density decays only by a factor of approximately 2, while the temperature decay is about an order of magnitude higher, as predicted.

So far, experimental evidence of evaporation cooling in a decaying plasma is provided and all predicted trends of the model are confirmed by the measurements. In Fig. 3 simulation results are shown for time domains where we do not have diagnostic access. A rather drastic change of the cooling rate becomes obvious when the electron temperature approaches the gas (ion) temperature. Thermalization occurs at earlier times than predicted by τ_β, since Coulomb collisions have a small but noticeable effect already at temperatures above the gas temperature, and τ_ε is not strictly a constant but decreases with temperature. The simulated temperature decay is clearly exponential, as demonstrated by the fit with a time constant of 15 ms. The value calculated by Eq. (13) using spatially averaged values from the simulation ($\langle T_g\rangle_V = 0.047$ eV, and $\langle\nu_{in}\rangle_V = 0.9 \times 10^5$ s^{-1}) is 17 ms, which is very close, especially in light of the approximations made in the derivation. The hypothetical final temperature is of course set by elastic collisions and follows from Eq. (5) as $kT_e^{(f)} = 2m_e\langle\nu_{in}\rangle_V\langle\nu_{en}\rangle_V l_d^2\gamma = 2.3 \times 10^{-4}$ eV (2.7 K), also in good agreement with simulation. However, then only very few charges remain. It is interesting to note that with the above scaling the plasma coupling parameter $g = 1/(n_e\lambda_D^3)$ [11] is proportional to $T_e^{-1/4}$. Therefore, it cannot rise much above the value reached at $T_e = T_g$, which is $g = 0.1$ in our case.

V. CONCLUSION

In summary, the analytical model, simulation, and experiment agree very well and a detailed insight into the physics providing quantitative description of electron evaporation cooling is presented together with the temporal evolution of electron temperature and density. It is found that in the late afterglow electrons thermalize primarily through Coulomb collisions with ions rather than elastic collisions with the neutrals. Evaporation is efficient only before thermalization. At lower temperatures the particle loss rate exceeds the cooling rate. Adoption of the model to other geometries is easy, and

extension to expanding plasmas, e.g., after short-pulse laser ionization, should be straightforward.

ACKNOWLEDGMENTS

We would like to thank Prof. J. Winter and Dr. M. Böke (Ruhr University Bochum) for providing the microwave interferometer. Support by the Alexander-von-Humboldt Foundation (Ts.V.Ts.), Nagoya University (M.A.), and the Graduate University for Advanced Studies (Sh.Y.) is gratefully acknowledged.

APPENDIX A

The validity of the following approximation is briefly discussed:

$$\left\langle \frac{e\Phi}{kT_e}\vec{\nabla}\cdot\vec{\Gamma}_e \right\rangle_V \approx \frac{e\Phi_c}{kT_e}\langle\vec{\nabla}\cdot\vec{\Gamma}_e\rangle_V. \tag{A1}$$

In this equation Φ_c is the potential in the plasma center. Using the continuity equation

$$\frac{\partial n_e}{\partial t} = -\vec{\nabla}\cdot\vec{\Gamma}_e \tag{A2}$$

and the Boltzmann relation

$$\frac{e\Phi}{kT_e} = \frac{e\Phi_c}{kT_e} + \ln\left(\frac{n_e}{n_c}\right), \tag{A3}$$

one obtains

$$\left\langle \frac{e\Phi}{kT_e}\vec{\nabla}\cdot\vec{\Gamma}_e \right\rangle_V = -\frac{e\Phi_c}{kT_e}\frac{\partial}{\partial t}\langle n_e\rangle_V - \frac{\partial}{\partial t}\left\langle n_e \ln\left(\frac{n_e}{n_c}\right)\right\rangle_V. \tag{A4}$$

Since the ratio n_e/n_c does not depend on time, this yields

$$\left\langle \frac{e\Phi}{kT_e}\vec{\nabla}\cdot\vec{\Gamma}_e \right\rangle_V = -\frac{\partial n_c}{\partial t}\left[\frac{e\Phi_c}{kT_e}\left\langle\frac{n_e}{n_c}\right\rangle_V + \left\langle\frac{n_e}{n_c}\ln\left(\frac{n_e}{n_c}\right)\right\rangle_V\right]. \tag{A5}$$

Relation (A1) follows from the above when the second term in the brackets on the right-hand side is neglected. This is justified since the maximal value of expressions of the type $|x\ln(x)|$ for $x \in [0,1]$ is $1/e \approx 0.37$, while the function is zero at both ends of the interval. At the same time the ratio $e\Phi_c/kT_e$ is well above 4, depending on the gas and the plasma dimensions. The relation between the two terms in the brackets is further elucidated in the one-dimensional case in Fig. 4.

It should also be noted that the approximation (A1) remains valid also for stationary discharges. In this case the justification follows the same line of reasoning with the exception that one has to replace $-\partial/\partial t$ with the ionization frequency ν_{iz}.

APPENDIX B

In this discussion, the calculation of the following expression,

$$G = \left\langle(\vec{\sigma}\cdot\vec{\Gamma}_e)\left(1+\frac{e\delta\Phi}{kT_e}\right)\right\rangle_A, \tag{B1}$$

is presented for the case of conducting and dielectric walls (with the normal vector $\vec{\sigma}$ pointing outward). This

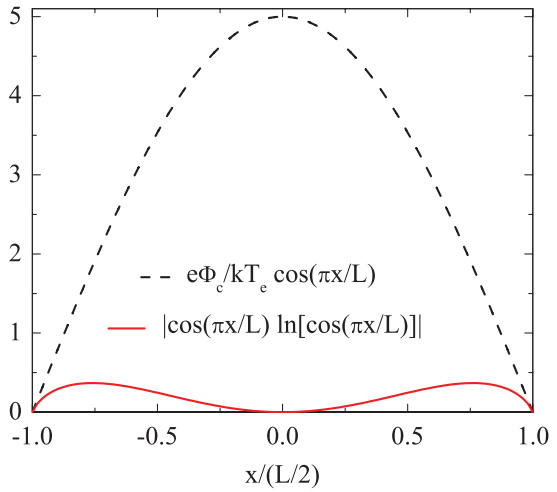

FIG. 4. (Color online) Comparison of the two functional dependencies on the distance of the two terms in (A5) for the case of $e\Phi_c/kT_e = 5$. The terms are proportional to the surface below the corresponding curves.

is the important step in obtaining Eq. (5) from Eq. (2). For the calculation, the three-dimensional diffusion electron density profile (4) is used together with the boundary condition (3).

Generally, the potential difference $\delta\Phi$ between the center and the walls can vary across the walls. However, in the case of conducting walls, the walls represent equipotential surfaces and $\delta\Phi = \text{const}$. Then the surface averaging extends over the electron flux only:

$$G = \langle\vec{\sigma}\cdot\vec{\Gamma}_e\rangle_A\left(1+\frac{e\delta\Phi}{kT_e}\right). \tag{B2}$$

Furthermore, the flux balance of charged particles is global: $\langle\vec{\sigma}\cdot\vec{\Gamma}_e\rangle_A = \langle\vec{\sigma}\cdot\vec{\Gamma}_i\rangle_A$. The surface-averaged ion flux is given by the Bohm flux $\langle\vec{\sigma}\cdot\vec{\Gamma}_i\rangle_A = u_B\langle n_B\rangle_A$, where u_B is constant due to the homogeneous electron temperature. Using Eq. (3) the surface-averaged Bohm flux is calculated to be

$$\langle\vec{\sigma}\cdot\vec{\Gamma}_e\rangle_A = u_B\langle n_B\rangle_A = \frac{4}{\pi}\frac{D_a n_c}{L}. \tag{B3}$$

On the other hand, the electron flux to the walls is determined by the thermal flux:

$$\langle\vec{\sigma}\cdot\vec{\Gamma}_e\rangle_A = \tfrac{1}{4}v_{th}\langle n_w\rangle_A. \tag{B4}$$

The electron density on the walls n_w is given by the Boltzmann factor and is constant for equipotential (metal) walls:

$$n_w = n_c\exp\left(-\frac{\delta\Phi}{kT_e}\right) = \text{const}. \tag{B5}$$

Combining (B3), (B4), and (B5) results in

$$\frac{e\delta\Phi}{kT_e} = \ln\left(\frac{\pi L v_{th}}{16D_a}\right) = \ln\left(\frac{Lv_{th}}{16D_a}\right) + \ln(\pi). \tag{B6}$$

This leads to the following expression for G in the case of conducting walls:

$$G = \frac{4}{\pi}\frac{D_a n_c}{L}\left[2 + \ln\left(\frac{L v_{th}}{16 D_a}\right) + c_w\right], \tag{B7}$$

with $c_w = \ln(\pi) - 1$.

Now the case of insulating dielectric walls is considered. In this case no conductive flux exists along the walls and the flux balance is required locally: $\vec{\sigma}\cdot\vec{\Gamma}_e = \vec{\sigma}\cdot\vec{\Gamma}_i$. Then the potential difference $\Phi_B - \Phi_w$ between the Bohm point and the walls, i.e., the floating potential, is homogeneous:

$$-\frac{e(\Phi_B - \Phi_w)}{kT_e} = \ln\left(\frac{n_w}{n_B}\right) = \ln\left(\frac{4u_B}{v_{th}}\right) = \text{const.} \tag{B8}$$

Therefore, $\delta\Phi$ can no longer be constant and is also subject to the surface averaging. Decomposing $\delta\Phi$ into the potential difference between the plasma center and the sheath edge (the Bohm point) and the potential difference between the Bohm point and the wall,

$$\delta\Phi = (\Phi_c - \Phi_w) = (\Phi_c - \Phi_B) + (\Phi_B - \Phi_w), \tag{B9}$$

allows (B1) to be rewritten as

$$G = \langle\vec{\sigma}\cdot\vec{\Gamma}_e\rangle_A\left[1 + \frac{e(\Phi_B - \Phi_w)}{kT_e}\right] + \left\langle(\vec{\sigma}\cdot\vec{\Gamma}_e)\left[\frac{e(\Phi_c - \Phi_B)}{kT_e}\right]\right\rangle_A. \tag{B10}$$

Using the Boltzmann relation and the local flux balance, the second term on the right-hand side becomes

$$\left\langle(\vec{\sigma}\cdot\vec{\Gamma}_e)\left[\frac{e(\Phi_c - \Phi_B)}{kT_e}\right]\right\rangle_A = u_B\left\langle n_B \ln\left(\frac{n_c}{n_B}\right)\right\rangle_A = n_c u_B\left\langle\frac{n_B}{n_c}\ln\left(\frac{n_c}{n_B}\right)\right\rangle_A. \tag{B11}$$

Using the boundary condition (3) with the density profile (4) to determine the Bohm density n_B leads to six identical integrals of the type

$$I = \int_{-L/2}^{L/2}\int_{-L/2}^{L/2}\cos\left(\pi\frac{x}{L}\right)\cos\left(\pi\frac{y}{L}\right) \times \ln\left[\cos\left(\pi\frac{x}{L}\right)\cos\left(\pi\frac{y}{L}\right)\right]dx\,dy = \frac{8L^2}{\pi^2}\left[\ln(2) - 1\right]. \tag{B12}$$

Finally one obtains

$$\left\langle(\vec{\sigma}\cdot\vec{\Gamma}_e)\left[\frac{e(\Phi_c - \Phi_B)}{kT_e}\right]\right\rangle_A = n_c\frac{4D_a}{\pi L}\left[\ln\left(\frac{4\pi D_a}{u_B L}\right) - 2\right]. \tag{B13}$$

Substituting the above result together with (B3) and (B8) in (B10) produces the result for dielectric walls:

$$G = \frac{4}{\pi}\frac{D_a n_c}{L}\left[2 + \ln\left(\frac{L v_{th}}{16 D_a}\right) - c_w\right]. \tag{B14}$$

[1] L. Spitzer, Jr., *Dynamical Evolution of Globular Clusters* (Princeton University Press, Princeton, NJ, 1987).
[2] H. F. Hess, Phys. Rev. B **34**, 3476 (1986).
[3] K. B. Davis, M. O. Mewes, M. R. Andrews, N. J. van Druten, D. S. Durfee, D. M. Kurn, and W. Ketterle, Phys. Rev. Lett. **75**, 3969 (1995).
[4] O. J. Luiten, M. W. Reynolds, and J. T. M. Walraven, Phys. Rev. A **53**, 381 (1996).
[5] M. A. Biondi, Phys. Rev. **93**, 1136 (1954).
[6] R. A. Gottscho, Bull. Am. Phys. Soc. **56**, 46 (2011).
[7] R. R. Arslanbekov and A. A. Kudryavtsev, Phys. Rev. E **58**, 7785 (1998); R. R. Arslanbekov, A. A. Kudryavtsev, and L. D. Tsendin, *ibid.* **64**, 016401 (2001); V. I. Kolobov and R. R. Arslanbekov, IEEE Trans. Plasma Sci. **34**, 895 (2006).
[8] A. Maresca, K. Orlov, and U. Kortshagen, Phys. Rev. E **65**, 056405 (2002); A. K. Bhattacharya and J. H. Ingold, J. Appl. Phys. **43**, 1535 (1972).
[9] V. A. Godyak and V. I. Demidov, J. Phys. D: Appl. Phys. **44**, 233001 (2011); **44**, 269501(E) (2011).
[10] E. W. McDaniel and E. A. Mason, *The Mobility and Diffusion of Ions in Gases* (John Wiley & Sons, New York, 1973).
[11] J. A. Bittencourt, *Fundamentals of Plasma Physics*, 3rd ed. (Springer, New York, 2004).
[12] O. Zatsarinny and K. Bartschat, J. Phys. B: At. Mol. Opt. Phys. **37**, 4693 (2004).
[13] H. A. Claaßen, Z. Naturforsch. A **28a**, 1875 (1973).
[14] K.-U. Riemann, J. Phys. D: Appl. Phys. **24**, 493 (1991).
[15] D. Rapp and P. Englander-Golden, J. Chem. Phys. **43**, 1464 (1965).
[16] L. Vriens and A. H. M. Smeets, Phys. Rev. A **22**, 940 (1980).
[17] A. Bohle and U. Kortshagen, Plasma Sources Sci. Technol. **3**, 80 (1994).
[18] PHELPS Database, [http://www.lxcat.laplace.univ-tlse.fr] (2012).
[19] C. M. Ferreira, J. Loureiro, and A. Ricard, J. Appl. Phys. **57**, 82 (1985).
[20] L. Spitzer, *Physics of Fully Ionized Gases*, 2nd ed. (Interscience, New York, 1962).
[21] Y. Celik, M. Aramaki, D. Luggenhölscher, and U. Czarnetzki, Plasma Sources Sci. Technol. **20**, 015022 (2011).
[22] A. Brockhaus, G. F. Leu, V. Selenin, Kh. Tarnev, and J. Engemann, Plasma Sources Sci. Technol. **15**, 171 (2006).
[23] D. Gahan, B. Dolinaj, and M. B. Hopkins, Rev. Sci. Instrum. **79**, 033502 (2008).